

# Finite Element Analysis of Tungsten Inert Gas Welding Temperatures on the Stress Profiles of AISI 1020 Low Carbon Steel Plate

Owunna Ikechukwu<sup>\*‡</sup>, Ikpe Aniekan E.<sup>\*\*</sup>

<sup>\*‡</sup>Department of Mechanical Engineering, University of Benin, Nigeria.

<sup>\*\*</sup>Department of Mechanical Engineering, University of Benin, Nigeria.

(ikechukwu.owunna@uniben.edu, aniekan.ikpe@eng.uniben.edu)

<sup>‡</sup>Corresponding Author; Owunna I., Room 142, Department of Mechanical Engineering, University of Benin, Nigeria.

Tel: +2349034983495, ikechukwu.owunna@uniben.edu

*Received: 06.03.2018 Accepted: 27.04.2019*

**Abstract-** For better understanding of the residual stress fields associated with Tungsten Inert Gas (TIG) welding, thermal analysis was carried out using Solid Works 2017 version and ESI Visual-Environment 2016 version to compute the transient temperature profile due to welding thermal loading and resulting stress field in three categories namely; von-mises stress, axial stress and thermal stress. A range of welding temperatures including 1746°C, 1912°C, 2100°C, 2410°C and 2800°C were experimentally applied in the joining process of AISI 1020 low carbon steel plate of 10 mm thickness and a strain gauge indicator was used to measure the thermal stresses induced in the steel plate which the average was recorded as 38,200MPa. The experimental parameters and conditions were applied in finite element simulation of the same plate dimension, and average von-mises stress of 37,508 MPa, average axial stress of 30,732 MPa and average thermal stress of 20,101 MPa was obtained. However, it was observed that the higher the welding temperature, the higher the stresses induced in the welding material. Hence, temperature for TIG welding process should be regulated at its optimum to avoid fatigue acceleration, stress propagation, early crack nucleation and possible fracture on the welded component which may limit the longevity and performance of such component in its service condition.

**Keywords:** TIG Welding, Induced stresses, Welding Temperature, Mild Steel, Finite Element Analysis.

## 1. Introduction

Welding is a process that involves joining two or more materials together, usually by melting the specimens into one piece and subsequent solidification of the melted parts [1]. Arc welding is divided into four (4) major processes such as Shielded Metal Arc Welding (SMAW) also known as Manual Metal Arc Welding, Gas Metal Arc Welding (GMAW) also known as Metal Inert Gas or Active Gas Welding (MIG/MAG), Flux Core Arc Welding (FCAW) and Gas Tungsten Arc Welding or Tungsten Inert Gas (TIG) which is the centre of focus in this paper [2, 3].

Due to the high temperature and heat distribution on the material in the Heat Affected Zone (HAZ), phase

transformation in the melting zone as well as rapid cooling and solidification during TIG welding process, residual stresses and possible distortions are induced in the welded material as a result of thermal effects in the welding sequence [4, 5]. According to Kamble and Rao [6], heat distribution around the weldment usually can alter the chemical and mechanical properties which depends upon the chemical composition of the welded metal. Two methods are generally used in determining residual stresses, namely; experimental method and computer-based simulations method. Experimental methods is known to exist in two forms such as destructive and non-destructive methods of which diffraction methods are examples of non-destructive method [7].

In recent times, application of finite element analysis (FEA) in welding processes through computer-based simulation tools have proven to be more efficient and time saving, providing accurate results depending on the input data and significant reduction in simulation cost over experimental methods [8, 9]. Perhaps of even greater importance, is that computer-based simulations allow the user to better visualize the complex cause and effect relationship between the various welding parameters and the residual stresses induced on the weldment [10]. The application of welding operation on a material generally causes high tensile stresses, yield stresses, as well as compressive stresses in the welded metal. During service condition of the material, the thermally induced stresses on the weldment transforms to residual stresses which may result in premature failure of the welded components by causing fatigue acceleration, stress propagation, early crack nucleation and possible fracture [11].

However, residual stresses due to welding defects are trapped within the components microstructure which gradually accelerates, thereby, hampering the performance and longevity of such material in service condition. This implies that when an area of a welded component is under compressive residual stress, the neighbouring area equally suffers the effects of tensile residual stresses trapped within the weldment [12]. Although some components may not fail due to residual stresses, they can contribute immensely to stresses from external loads acting on such components. Hence, residual stresses usually tend to lessen the strength of the welded component in service condition [13]. Since welding residual stresses are primarily the result of volume

changes during solidification, the stresses can be expressed in terms of three principal stresses (acting on a flat plate); axial stress, thermal stress and von-mises stress, which are the major areas of focus in this paper.

## 2. Materials and Methods

Two low carbon steel materials of 10mm thickness 50 mm x 35 mm (length x width) each were prepared for welding. Abrasive material (sand paper) was used to smoothen the entire material to eliminate all possible coatings, corrosion or rust that may have accumulated on the material. Prior to welding, surface of the samples to be welded were chemically cleaned with acetone to eliminate surface contamination and welding was applied on the flat plates using the conditions in Table 1. The weld pole as a result of heat application on the fusion zone is shown in Fig 1.

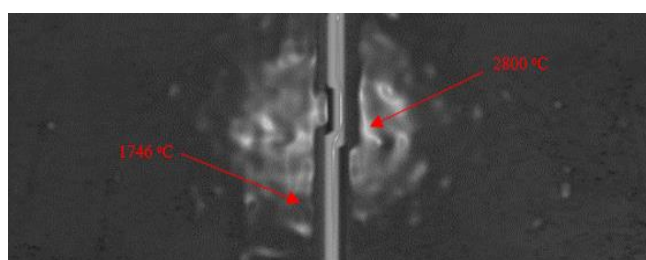


**Fig. 1.** Weld Pole of the Fusion Zone at Minimum and Maximum Temperature.

**Table 1.** Welding conditions applied in the TIG welding process

Tungsten Inert Gas	DCEN-Current	Welding Speed	Shielding Gas	Welding Power	Arc Voltage	Gas Flow Rate	Filler Rod Diameter
2.0L/min	130 A	0.18m/min	Pure argon	Alternating current (AC)	20V	20cfh	3/32

The welding runs were varied for different temperatures including 1746°C, 1912°C, 2100°C, 2410°C and 2800°C respectively as presented in Fig 2. As shown in Fig 3, P3 strain indicator was used to measure the residual stresses induced in the steel plate which the average was recorded as 38,200 MPa.



**Fig. 2.** Welded Samples showing Welding Temperatures

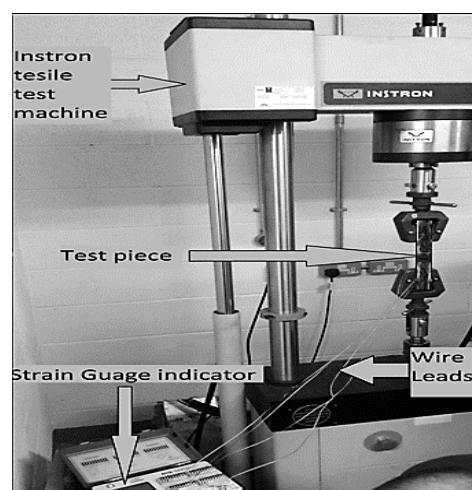


**Fig. 3.** Experimental Set-up showing the strain measurement

Using the available M-bond adhesive, rosette strain gauge was carefully and firmly applied at the back surface of the fusion zone on the test piece. Wire leads were soldered onto the nine terminals of the strain gauge rosette. This was carefully done

so as not to damage the strain gauge rosette. The stress values were obtained by multiplying the measured strain gauge values by the Young's modulus. However, visualization of thermally induced stress distributions on the material after the welding experimentation was complex. Considering the aforementioned welding parameters, computer-based simulations was conducted using Finite Element Analysis (FEA) to determine residual stress distribution and visualization across the material.

The FEA was carried out in two steps. A non-linear transient thermal analysis was initially conducted to obtain the global temperature profile generated during the welding process. Stress analysis was then developed with the temperatures obtained from the thermal analysis used as loading to the stress model. The FEA tool used to determine the von-mises stress was Solid Works 2017 version but the axial and thermal stresses were determined using ESI Visual-Environment. This is because Solid Works could only provide visuals of stress distribution on the welded parts, whereas, ESI Visual-Environment provided visuals of thermally induced stress distribution across the entire surface of the welded steel plate. Figure 4 represent temperature profile of the 10 mm mild steel plate in ESI Visual-Environment. Table 2 represents mechanical properties of the mild steel plate. The 3-D finite

element model of the plate took a longer mesh converging time in solid works due to the large number of nodes (108015). As an alternative, a 2-D axisymmetric model in ESI Visual-Weld was developed using quadratic meshing elements (shown in Table 3) with 1342 nodes in order to simplify the mesh converging time and computational speed.

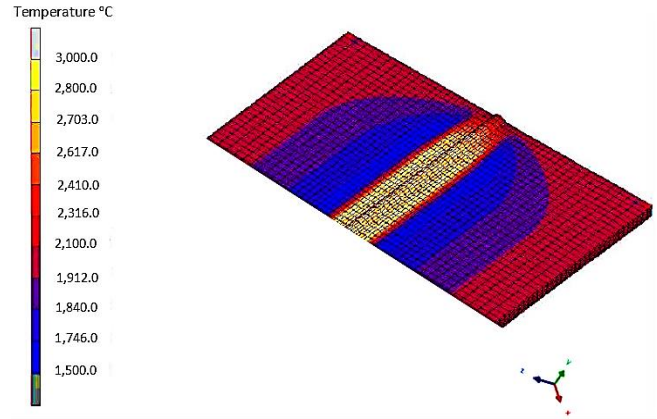


**Fig. 4.** Temperature Range Adopted for the FEA of 10 mm Mild Steel Plate

**Table 2.** Mechanical Properties of AISI 1020 Mild Steel plate

Material: AISI 1020	Properties	Model
Model type	Linear Elastic Isotropic	
Default failure criterion	Max von Mises Stress	
Yield strength	351.571 N/mm <sup>2</sup>	
Tensile strength	420.507 N/mm <sup>2</sup>	
Elastic modulus	200000 N/mm <sup>2</sup>	
Poisson's ratio	0.29	
Mass density	7900 g/cm <sup>3</sup>	
Shear modulus	77000 N/mm <sup>2</sup>	
Thermal expansion coefficient	1.5e-005 /Kelvin	

**Table 3.** Solid Works-Solid mesh and ESI Visual-Mesh Visualization

Solid Works-Solid mesh, 108015 nodes	ESI Visual-Mesh, 1342 nodes

**3. Thermal Analysis**

During Tungsten Inert Gas welding process, the heat input per unit of time is given by equation 1;

$$\dot{Q} = \eta UI \tag{1}$$

where  $U$  is the voltage,  $I$  is the current and  $\eta$  is the arc efficiency.

Heat transfer in welding process is a non-linear condition due to the dependence of the material's thermos-physical properties on temperature. However, residual stresses and distortions are produced as a result of heterogeneous welding temperature caused by localized heat input during the welding

process. In this case, tungsten electrode is the heat source in which the state of heat transfer is given by equation 2.

$$\rho c \frac{\partial T}{\partial t} = \frac{\partial}{\partial x} \left( k \frac{\partial T}{\partial x} \right) + \frac{\partial}{\partial y} \left( k \frac{\partial T}{\partial y} \right) + \frac{\partial}{\partial z} \left( k \frac{\partial T}{\partial z} \right) + Q \quad (2)$$

Where  $p$  is the density,  $c$  is the specific heat capacity,  $k$  is the thermal conductivity coefficient and  $Q$  is the heat flux.

The heat source equation for first half of the mild steel plate is given by equation (3);

$$q(x, y, z, t) = \frac{6\sqrt{3Qf_f}}{abc_1\pi\sqrt{\pi}} e^{-3\left(\frac{x^2}{a^2} + \frac{y^2}{b^2} + \frac{(z-vt)^2}{c_1^2}\right)} \quad (3)$$

The heat source equation for the second half of the mild steel plate is given by equation (4);

$$q(x, y, z, t) = \frac{6\sqrt{3Qf_r}}{abc_2\pi\sqrt{\pi}} e^{-3\left(\frac{x^2}{a^2} + \frac{y^2}{b^2} + \frac{(z-vt)^2}{c_2^2}\right)} \quad (4)$$

Where  $q$  is the total heat source,  $v$  is the welding speed  $f_f$  and  $f_r$  are the energy fraction of the heat source,  $a$ ,  $b$ , and  $c$  is the half axle in different directions,  $t$  is the thickness of the plate.

Heat losses on the workpiece surfaces by convection,  $q_c$ , and radiation,  $q_r$ , are introduced as boundary conditions, given by equation (5) and (6) respectively [14].

$$q_c = h(T - T_\infty) \quad (5)$$

$$q_r = \delta S (T^4 - T_\infty^4) \quad (6)$$

Where  $h$  and is the convention coefficient,  $T_\infty$  is the temperature of the surrounding fluid,  $\delta$  is the Stefan-Boltzmann constant,  $S$  is the radiation area.

While modelling the plastic behaviour of a flat plate, it is important to define the elastic domain, which is usually based on the von Mises criterion derived from equation (7).

$$f = \sigma_v M - \sigma_y < 0 \quad (7)$$

Where  $f$  is the yielding function,  $\sigma_y$  is the material's yield stress and  $\sigma_v M$  is the von Mises equivalent stress, given by equation 8 respectively [15].

$$\sigma_v M = \left[ \frac{(\sigma_1 - \sigma_2)^2 + (\sigma_2 - \sigma_3)^2 + (\sigma_3 - \sigma_1)^2}{2} \right]^{\frac{1}{2}} \quad (8)$$

Where  $\sigma_1$ ,  $\sigma_2$  and  $\sigma_3$  are the principal stresses. According to the von Mises criterion, plastic strains will be developed when the condition in equation (7) is met.

In a typical welding process, there is heat source that provide the arc energy required for the operation, and this can cause localized increase in thermally induced stress as a result of the high temperature from the arc. To simulate the arc heating effect on the welded material, the equivalent heat input can be assumed as the combination of both the surface flux and body flux [16]. The surface flux  $q_s$  and body flux  $q_b$  are generally expressed as Gaussian distribution given by equation (9) and (10);

$$q_s = \frac{3Q_s}{\pi a c} \exp \left\{ -\frac{3x^2}{a^2} - \frac{3z^2}{c^2} \right\} \quad (9)$$

$$q_b = \frac{6\sqrt{3Q_b}}{abc\pi\sqrt{\pi}} \exp \left\{ -\frac{3x^2}{a^2} - \frac{3y^2}{b^2} - \frac{3z^2}{c^2} \right\} \quad (10)$$

Where  $a$ ,  $b$ , and  $c$  are the semi-characteristic arc dimensions in  $x$ ,  $y$ , direction.

#### 4. Results

Table 4 represents the work flow sensitivity sensors which is a platform in solid works simulation that allows the sensor to be used in any plot using probe tool which can equally probe the simulation results at various scenarios for accuracy. Table 5 extracted from the solid works transient analysis represents the reaction forces (N) at different welding Temperature ( $^{\circ}\text{C}$ ). In addition, the stress results obtained from different welding temperatures is presented in Table 6, while the plot of stress results obtained from different welding temperature intervals is indicated in Fig. 5, respectively. However, the stress distribution across the two welded metals were somewhat similar and followed almost the same distribution trend. Therefore, the stress results presented in this section are only shown for one half of the welded mild steel plates at various welding temperature as shown in Figs. 6-20. For better visualization of the axial and thermally induced stress propagation and distribution across one half of the welded metal particularly at the surface, the same mild steel plate was also simulated in ESI Visual-Environment.

**Table 4.** Workflow Sensitive Sensors at different Welding Temperature

Points	Locations (mm)	Normal X	Normal Y	Normal Z	Shear XY	Shear XZ	Shear YZ
Workflow Sensitive Sensors at 1746 $^{\circ}\text{C}$ (Stress Components - N/mm $^2$ (MPa))							
1	-5.2122, -15.3915, 14.6747	-12.72	643.50	-3.97	27.70	-3.53	3.90
2	-5.2122, -21.3290, 14.6747	-0.15	-1.34	-6.04	-0.16	-1.38	3.79
Workflow Sensitive Sensors at 1912 $^{\circ}\text{C}$ (Stress Components - N/mm $^2$ (MPa))							
1	-5.2122, -15.3915, 14.6747	-10.05	599.19	-3.19	26.51	-2.86	4.93
2	-5.2122, -21.3290, 14.6747	-0.26	-1.28	-5.38	-0.22	-1.28	3.34
Workflow Sensitive Sensors at 2100 $^{\circ}\text{C}$ (Stress Components - N/mm $^2$ (MPa))							
1	-5.2122, -15.3915, 14.6747	-17.57	915.29	-5.59	40.32	-4.82	5.67
2	-5.2122, -21.3290, 14.6747	-0.08	-2.07	-8.25	-0.26	-1.38	5.47
Workflow Sensitive Sensors at 2410 $^{\circ}\text{C}$ (Stress Components - N/mm $^2$ (MPa))							
1	-5.2122, -15.3915, 14.6747	-16.73	989.23	-5.65	43.99	-4.63	7.73

2	-5.2122, -21.3290, 14.6747	-0.07	-2.26	-8.54	-0.33	-1.38	5.70
Workflow Sensitive Sensors at 2800°C (Stress Components - N/mm <sup>2</sup> (MPa))							
1	-5.2122, -15.3915, 14.6747	-21.63	1303.54	-7.38	58.77	-5.94	10.35
2	-5.2122, -21.3290, 14.6747	-0.01	-3.16	-11.07	-0.45	-1.38	7.56

**Table 5.** Reaction Forces (N) at different welding Temperature (°C)

Selection set	Welding Temperature (°C)	Sum X	Sum Y	Sum Z	Resultant
Entire Model	1746	0.0576439	1.39219	0.0337265	1.39379
	1912	0.039957	1.34291	-0.0314658	1.34387
	2100	-0.0282955	1.41269	0.0461736	1.41373
	2410	-0.0388947	1.40332	0.0240045	1.40406
	2800	0.0572472	1.43699	-0.0527453	1.4391

**Table 6.** Stress results obtained from different Welding Temperatures

Welding Runs	Welding Temperature (°C)	Max Experimental Thermal Stress (N/mm <sup>2</sup> )	Max Von-mises Stress (N/mm <sup>2</sup> )	Max Axial Stress (N/mm <sup>2</sup> )	Max Thermal Stress (N/mm <sup>2</sup> )
1	1,746	25,450	24,352.555	21,973.00	11,613.00
2	1,912	26,730	25,806.361	24,961.00	13,523.00
3	2,100	36,060	35,471.488	30,834.00	18,720.00
4	2,410	43,490	43,681.516	35,387.00	25,790.00
5	2,800	59,270	58,229.234	40,507.00	30,863.00
Average	2,194	38,200	37,508.2	30,732	20101.8

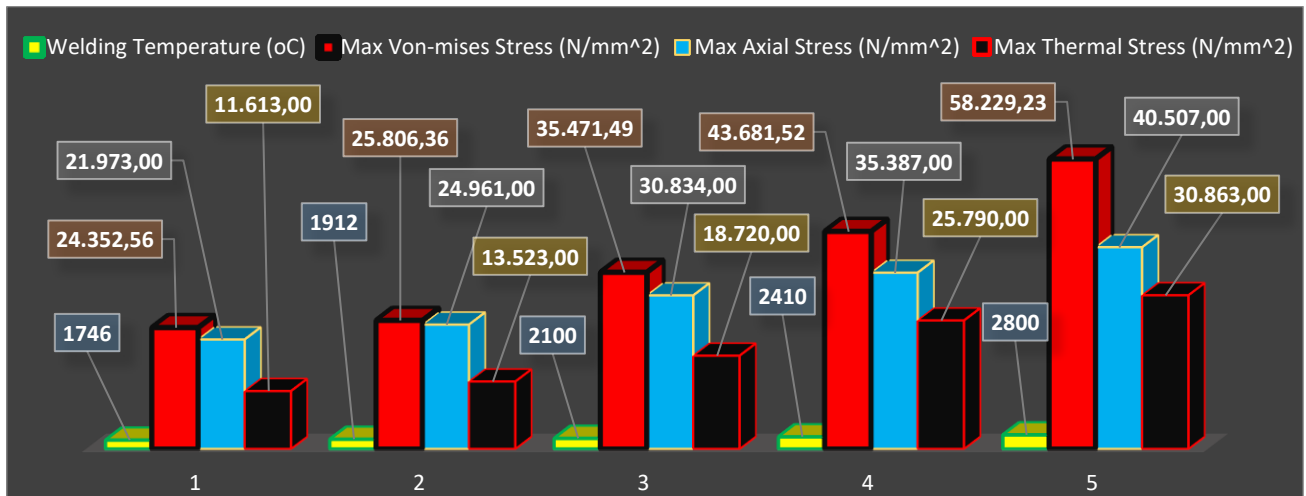


**Fig. 5.** Plot of Stress results obtained from different Welding Temperature Intervals

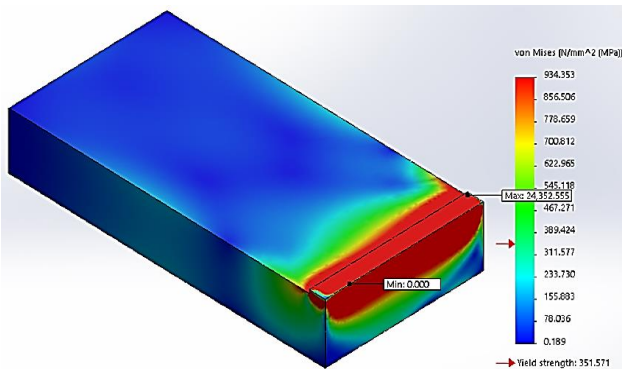


**Fig. 6.** Von-mises stress distribution Profile from solid Works at 1746°C

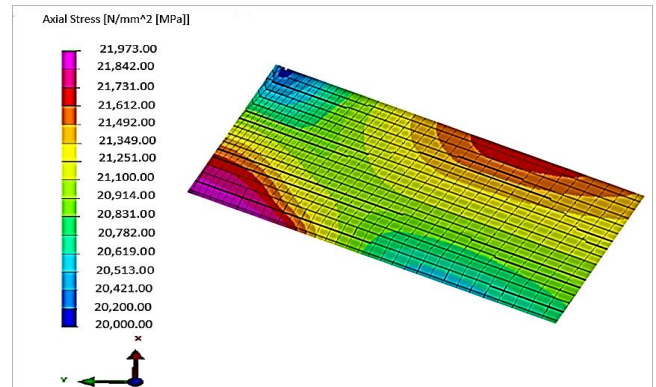


**Fig. 7.** Axial stress distribution Profile from ESI-Visual at 1746°C

The thermally induced stresses in the fusion zone of the welded metal may be due to the welding parameters. This has been indicated in several studies carried out in recent times. For example, Owunna and Ikpe (2018) [17] reported that the hardness property of a welded metal can be affected by the Welding voltage, while the strength of the weld joints can improve with decreasing welding voltage but prone to thermal stress at increasing welding current. The higher welding amperage in effect can result in undercut due to welding operations conducted with relatively high amperage or relatively long arc length which would leave a groove in the base metal along either sides of the bead, thereby, causing residual stress build-up and reduction in the strength of the weldment [18]. It was observed in similar studies that excessively high welding temperature and voltage can result in a wider bead that would subject the weldment to thermal stress cracking, increased undercut, increased side wall fusion defects and difficulty in slag removal while amperage set too low may result in a narrow and erratic beads that would affect fusion of the metal plates [19].

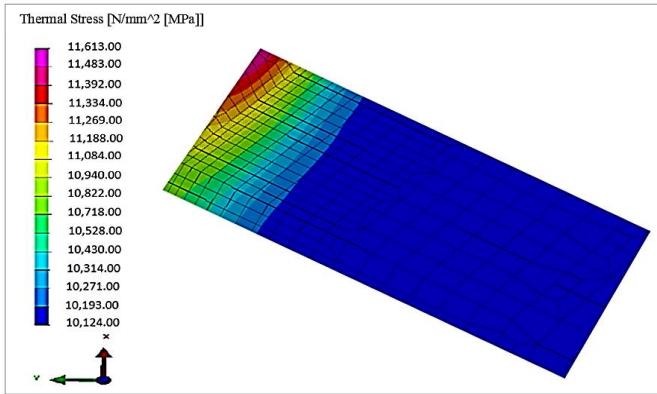


**Fig. 8.** Thermal induced stress distribution Profile from ESI-Visual at 1746°C

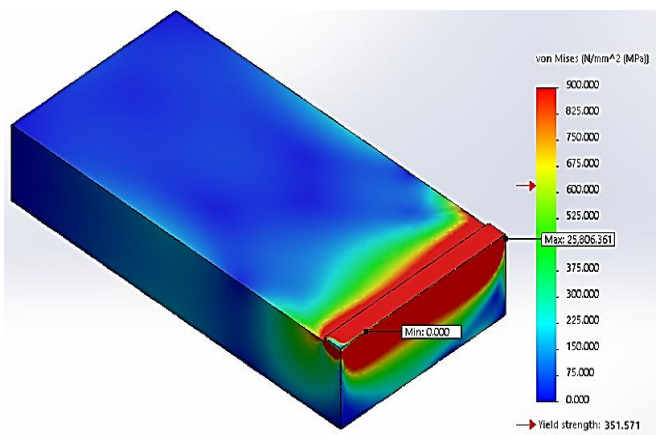


**Fig. 9.** Von-mises Stress Distribution Profile from Solid Works at 1912°C

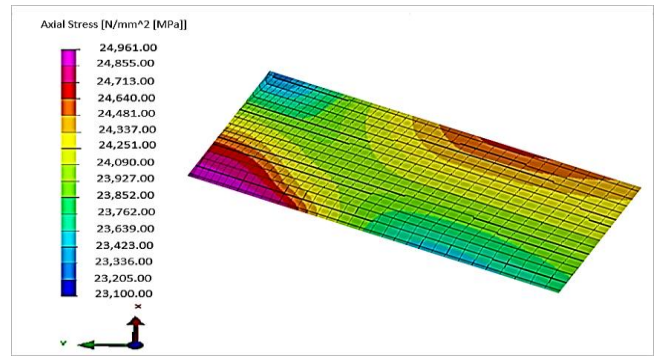


**Fig. 10.** Axial stress distribution Profile from ESI-Visual at 1912°C

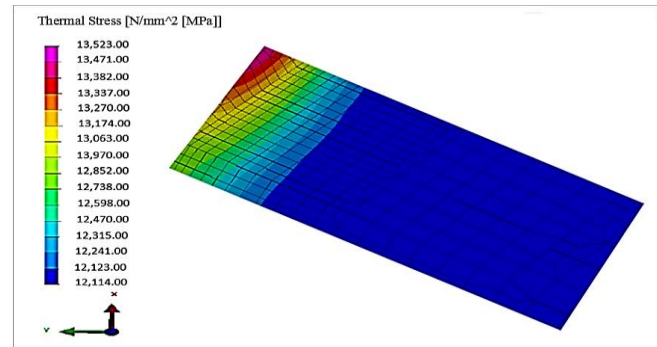


**Fig. 11.** Thermal stress distribution Profile from ESI-Visual at 1912°C

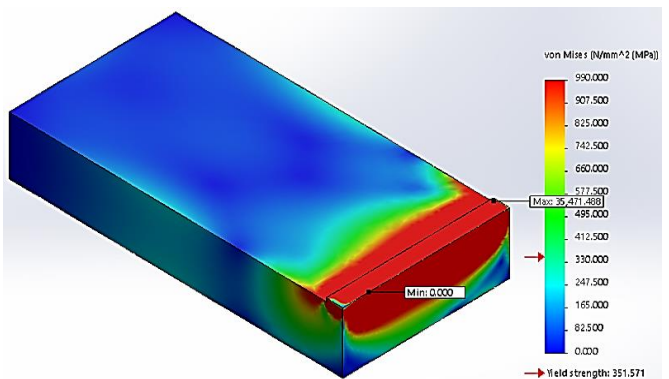


**Fig. 12.** Von-mises Stress Distribution Profile from Solid Works at 2100°C

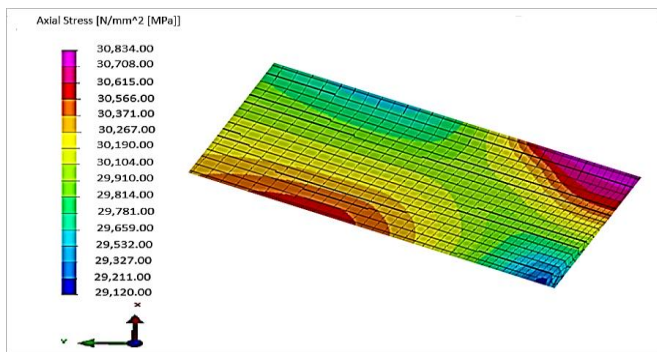


**Fig. 13.** Axial stress distribution Profile from ESI-Visual at 2100°C

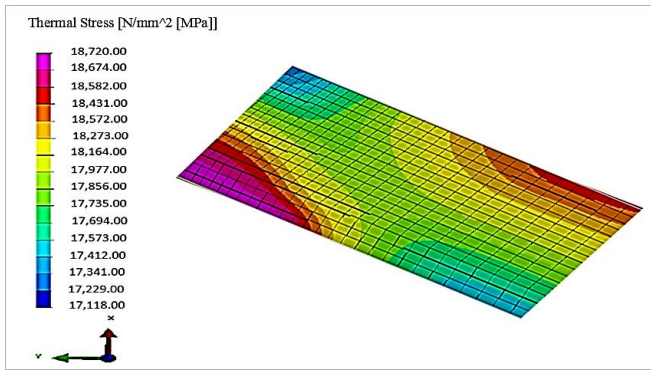


**Fig. 14.** Thermal stress distribution Profile from ESI-Visual at 2100°C

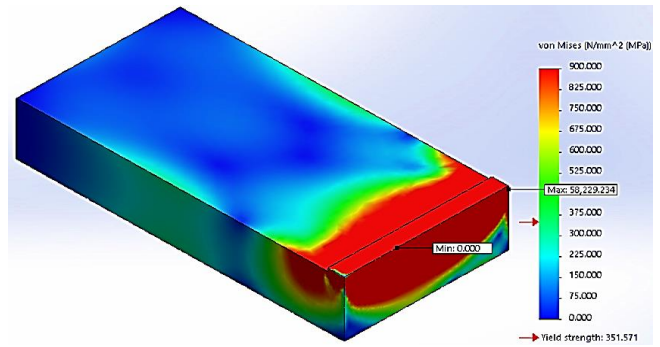


**Fig. 18.** Von-mises Stress Distribution Profile from Solid Works at 2800°C

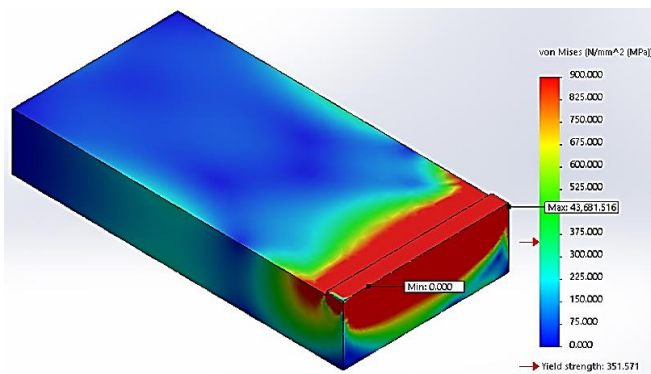


**Fig. 15.** Von-mises Stress Distribution Profile from Solid Works at 2410°C

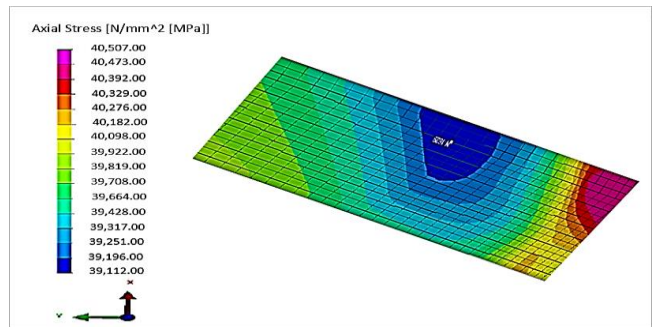


**Fig. 19.** Axial stress distribution Profile from ESI-Visual at 2800°C

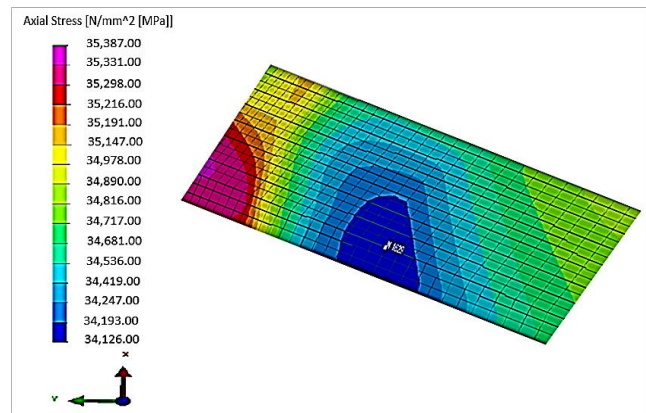


**Fig. 16.** Axial stress distribution Profile from ESI-Visual at 2410°C

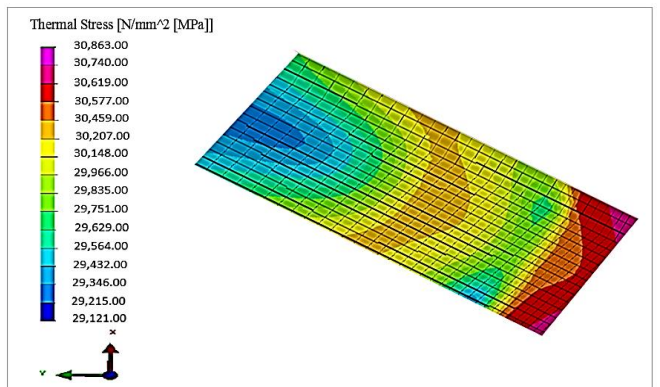


**Fig. 20.** Thermal stress distribution Profile from ESI-Visual at 2800°C

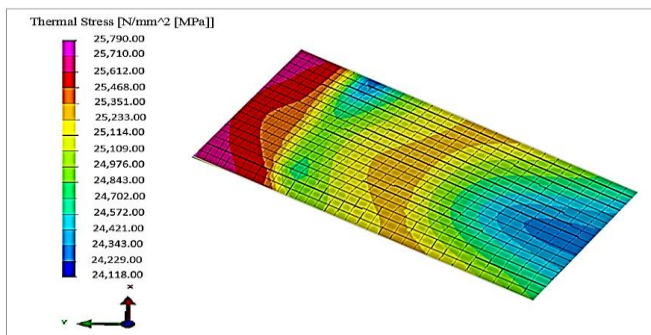


**Fig. 17.** Thermal stress distribution Profile from ESI-Visual at 2410°C

Table 6 best exemplify this phenomenon where welding temperature of 1746°C yielded maximum von-mises stress of 24,352.555 MPa, maximum axial stress (tensile stress) of 21,973.00 MPa and maximum thermal stress of 11,613.00 MPa. Furthermore, increasing the welding temperature to 1912°C led to increased maximum von-mises stress of 25,806.361 MPa, maximum axial stress of 24,961.00 MPa and maximum thermal stress of 13,523.00 MPa while further increase in the welding temperature to 2100°C produced increasing maximum von-mises stress of 35,471.488 MPa, maximum axial stress of 30,834.00 MPa and maximum thermal stress of 18,720.00 MPa respectively. In addition, the last two welding temperature was increased to 2410°C and 2800°C and maximum von-mises stress of 43,681.516 MPa, maximum axial stress of 35,387.00 MPa, maximum thermal

stress of 25,790.00 MPa and maximum von-mises stress of 58,229.234 MPa, maximum axial stress of 40,507.00 MPa, maximum thermal stress of 30,863.00 MPa. The Solid Works models shown in Figs. 6, 9, 12, 15 and 18 were simulated to determine the von-mises stress but visuals of the stress distributed across the welded material showed that the stress concentrated mainly on the weldment and edges of the welded metal, whereas, visuals of the stress distribution on the surface of the metal plate were more elaborate with ESI Visual-Environment as shown in Fig 7, 8, 10, 11, 13, 14, 16, 17, 19 and 20 respectively.

The high temperature around the welding pool and the existing heat dissipation through the plate and from the surface cause a severe temperature gradient across the welded material and possible stresses that may alter the microstructure of the material, as the HAZ extends from the welded joint. According to Owunna and Ikpe [20], heat distribution around the weldment usually alters the chemical and mechanical properties which depends upon the chemical composition of the bead and its geometry. This is in agreement with the studies on weld bead penetration in Tungsten TIG welding of AISI 1020 low carbon steel plate, where it was observed that higher the temperature distribution across the fusion zone, the wider the Heat Affected Zones (HAZs) which are indications of phase transformations and alterations in mechanical properties of the welded metal which may lead to induced residual stresses if the welding parameters particularly the amperage is not controlled adequately [21].

As shown in Fig. 5, the induced stresses were computed in three categories namely; Von-mises yield criterion (also referred to as maximum distortion energy criterion) which is part of plasticity theory for ductile materials, suggesting that the yielding effect of a given material commences when the second deviatoric stress invariant reaches a critical value. In other words, von-mises stress is a value that can be used to determine the rate of yield or fracture in a material. The second category of stress considered in this study is tensile stress which tends to alter the length of a body by causing the welded material to elongate in the direction of the applied welding force, whereas the third category of stress considered in this study is the thermal stress which is induced in the welded material due to temperature variation, thermal expansion or contraction and thermal shocks, and can result in fracture or plastic deformation depending on the heat constraint and other variables such as thermal conductivity of the material.

Generally, thermal stress is a constraint that significantly affect a material subjected to high temperature welding condition, and it is highly dependent on the thermal expansion coefficient of the welded material. In other words, the higher the temperature variation, the higher the stresses induced in the welded material as tabulated earlier in Table 6. This correlates with the investigation carried out by Tarak [10] on residual stresses due to circumferential girth welding of austenitic stainless steel pipes.

## 5. Conclusion

Based on the objective of this work, a Finite Element Method based on transient thermal elastic plastic model was developed and the effects of TIG welding cycle on AISI 1020 low carbon steel plate of 10 mm thickness was examined. The material parameters for the AISI 1020 mild steel were assumed to be temperature dependent, while other constraints such as distributed arc heat input, heat loss, welding speed, shielding gas, welding power, arc voltage, gas flow rate were considered in the model. From the stresses obtained from the thermal transient analysis of TIG welding process of mild steel in this study, it has been observed that temperature gradient in terms of heat input plays a major role in welding in which lower heat input affects the quality of the welded joints. Therefore, optimum heat input is ideal for joining of two or more metals together. In addition, comparing the results obtained for each of the three average stress (maximum von-mises stress, maximum axial stress and maximum thermal stress) categories and the maximum average stress result measured with a strain gauge indicator during the experimental exercise showed relatively less difference for von-mises stress (692 Mpa), a higher difference in terms of axial stress (7,468 MPa) and relatively high difference in thermal stress (18,099 MPa), thus, indicating that thermal induced stress which is a function of high temperature and heat input during welding operation must be prerequisite for consideration prior to commencement of any welding operation.

## References

- [1] K. Y. Benyounis and A. G. Olabi, "Optimization of Different Welding Process Using Statistical and Numerical Approaches: A Reference Guide", Advanced Engineering Software, Vol. 39, pp. 483-496, 2008.
- [2] K. Weman, Welding processes handbook. New York: CRC Press LLC. ISBN 0849317738, 2003.
- [3] A. E. Ikpe, I. Owunna and I. Ememobong, "Effects of Arc Voltage and Welding Current on the Arc Length of Tungsten Inert Gas Welding (TIG)" International Journal of Engineering Technologies-IJET, Vol. 3, Issue 4, pp. 213-221, 2017.
- [4] R. K. Jain, Production Technology, Khanna Publishers, New Delhi pp. 344-346, 2001.
- [5] N. Sura, and V. Mittal, "Experimental Study on Effects of Process Parameters on HAZ of Plain Carbon Steel Using GMAW", International Journal of Latest Research in Science and Technology, Vol. 4, Issue 2, pp. 167-170, 2015.
- [6] A. G. Kamble and R. V. Rao, "Experimental Investigation on the Effects of Process Parameters of GMAW and Transient Thermal Analysis of AISI 321 Steel", Advances in Manufacturing, Vol. 1 Issue 4, pp. 362-377, 2013.
- [7] E. Lima, J. Wagener, A. Pyzalla and T. Buslaps, "Investigations on Residual Stresses in Friction Stir

- Welds", in 3rd International Symposium on Friction Stir Welding, Kobe, Japan, 2001.
- [8] M. V. Dalvi, A. S. More, S. P. Joshi and V. M. Junnarkar, "Determination of Failure Strength of Flat Plate Weld Joint Using Finite Element Analysis", *International Journal of Scientific & Engineering Research*, Vol. 3, Issue 12, pp. 302-306, 2012.
- [9] C. S. Baviskar, R. M. Tayade and V. G. Patil, "Determination of Failure Strength of Curved Plate Weld Joint Using Finite Element Analysis", *International Journal of Mechanical Engineering and Robotic Research* Vol. 1 Issue 3, 22-30, 2012.
- [10] F. Tarak, *Residual Stresses Due to Circumferential Girth Welding of Austenitic Stainless Steel Pipes*, Theses and Dissertations, Paper 1649, Lehigh University, 2013.
- [11] M. Law, H. Prask, V. Luzin and T. Gnaeupel-Harold, *Residual stress measurements in coil, linepipe and girth welded pipe*, Elsevier Science Ltd., Menai, 2006.
- [12] G. Mi, C. Li, Z. Gao, D. Zhao and J. Niu, "Finite Element Analysis of Welding Residual Stress of Aluminium Plates Under Different Butt Joint Parameters" *Engineering Review*, Vol. 34, Issue 3, 161-166, 2014.
- [13] L. Karlsson, *Residual Stresses Due to Welding of a Nozzle to a Pressure Vessel*, Lund University, Lund, 2005.
- [14] T. D. Eastop and A. McConkey, *Applied Thermodynamics for Engineering Technologist*, Fourth Edition, Pearson Education Ltd. ISBN: 8178085577, 2004.
- [15] R. G. Budynas and J. K. Nisbett, *Shigley's Mechanical Engineering Design*, 9th Edition, McGraw-Hill Higher Education: New York, 2011.
- [16] B. I. Bang, Y. P. Son, K. H. Oh, Y. P. Kim and W. S. Kim, "Numerical simulation of sleeve repair welding of in-service gas pipelines", *Welding Journal*, Vol. 81, pp. 273-282, 2002.
- [17] I. B. Owunna, and A. E. Ikpe "Effects of Parametric Variations on Bead Width of Gas Tungsten Arc Welding of AISI 1020 Low Carbon Steel Plate", *International Journal of Engineering Technology and Sciences*", Vol. 5, Issue 3, pp. 1-13, 2018.
- [18] I. Owunna, A. E. Ikpe and J. I. Achebo, "Temperature and Time Dependent Analysis of Tungsten Inert Gas Welding of Low Carbon Steel Plate using Goldak Model Heat Source", *Journal of Applied Science and Environmental Management*, Vol. 22, Issue 11, pp. 1719-1725, 2018.
- [19] Ikpe A. E. and I. Owunna, "Optimization of TIG Welding Input Variables for AISI 1020 Low Carbon Steel Plate Using Response Surface Methodology", *International Journal of Engineering Science and Application*, Vol. 2, Issue 3, pp. 113-122, 2018.
- [20] I. B. Owunna and A. E. Ikpe, "Modelling and Prediction of the Mechanical Properties of TIG Welded Joint for AISI 4130 Low Carbon Steel Plates Using Artificial Neural Network (ANN) Approach", *Nigerian Journal of Technology*, Vol. 38, Issue 1, pp. 117-126, 2019.
- [21] I. Owunna, A. E. Ikpe and J. I. Achebo, "3D Finite Element Modelling of Weld Bead Penetration in Tungsten Inert Gas (TIG) Welding of AISI 1020 Low Carbon Steel Plate", *European Mechanical Science*, Vol. 2, Issue 3, pp. 96-105, 2018.